JOURNAL OF GEOPHYSICAL RESEARCH, VOL. 100, NO. B4, PAGES 6265–6280, APRIL 10, 1995

The 1946 Hispaniola earthquakes and the tectonics of the North America-Caribbean plate boundary zone, northeastern Hispaniola

R. M. Russo[1]

Department of Terrestrial Magnetism, Carnegie Institution of Washington, Washington, D.C.

A. Villaseñor

Instituto de Ciencias de la Tierra (Jaume Almera), Barcelona, Spain

Abstract. We have determined focal mechanisms for the largest earthquake ($M_S = 7.8$) recorded instrumentally in the Caribbean Basin, the August 4, 1946, Hispaniola earthquake, and three of its large-magnitude ($M_S \geq 6.1$) aftershocks. We also relocated 63 aftershocks and one foreshock of the event series. The aftershock series is elongate, trends WNW, and is centered on the Samaná Peninsula of northeast Hispaniola. Shallow aftershocks are in a 75-km-wide linear zone, and intermediate depth (70 to 130 km) aftershocks apparently delineate a moderately south or SSW dipping slab. It is not clear, however, whether these events indicate active subduction of North American Atlantic Ocean lithosphere or are strike-slip events on the interface between subducted but no longer sinking slab and Caribbean mantle. We constrained focal mechanisms of the main shock and three aftershocks by combining observed P and S polarities and amplitude ratios and also by waveform modeling. The two methods yield consistent results. The mechanisms include strike-slip and thrust displacements on NW striking nodal planes. Fault dip is variable, NE or SW. The NW striking fault planes parallel mapped terrane boundaries and faults in the North America (NA)-Caribbean (Ca) plate boundary zone and are also parallel to the aftershock series trend. We interpret the events to be motions on a WNW trending restraining bend segment of the NA-Ca plate boundary in eastern Hispaniola. We have calculated magnitudes for eight of the earthquakes in the series; for the three events (including the main shock) for which data are available, our magnitudes are systematically less than the previously published magnitude estimates. Given the high magnitude and large aftershock area of the August 4, 1946, event, these earthquakes probably represent the true long-term interplate motions between North America and the terranes in this portion of the plate boundary zone.

Introduction

Tectonic and geologic complexity and slow plate motion rates are the hallmarks of the eastern Caribbean (Ca)-North America (NA) plate boundary zone (Figure 1a) [*Molnar and Sykes,* 1969; *DeMets et al.,* 1990; *Lewis and Draper,* 1990]. Better determination of plate and microplate motions in this region is highly desirable because the earthquake slip vectors [*Sykes et al.,* 1982] and transform fault azimuths [*Jordan,* 1975; *DeMets et al.,* 1990] from this plate boundary zone yield discordant velocities of the Caribbean plate relative to North America. Furthermore, the slow motions along this plate boundary zone require that such study encompass the longest time period possible, in order to assess accurately the full range of seismogenic displacements and recurrence times. Enhanced knowledge of the loci of currently active seismogenic fault zones, and of the types of motions on these faults, is also important in mitigating seismic hazard to the large and growing populations of the Greater Antilles. In an attempt to address these issues, we have studied the August 4, 1946 earthquake and its aftershocks. This event is the largest magnitude earthquake ($M = 8.1$ [*Gutenberg and Richter,* 1954] to have occurred in the Caribbean basin during the period of instrumental recording of seismicity (1899 to present). As such it is particularly important to understand its source mechanism and the tectonic motions it represents.

[1]Now at Laboratoire de Tectonophysique, Université de Montpellier II, Montpellier, France.

Paper number 94JB02599.
0148-0227/95/94JB-02599$05.00

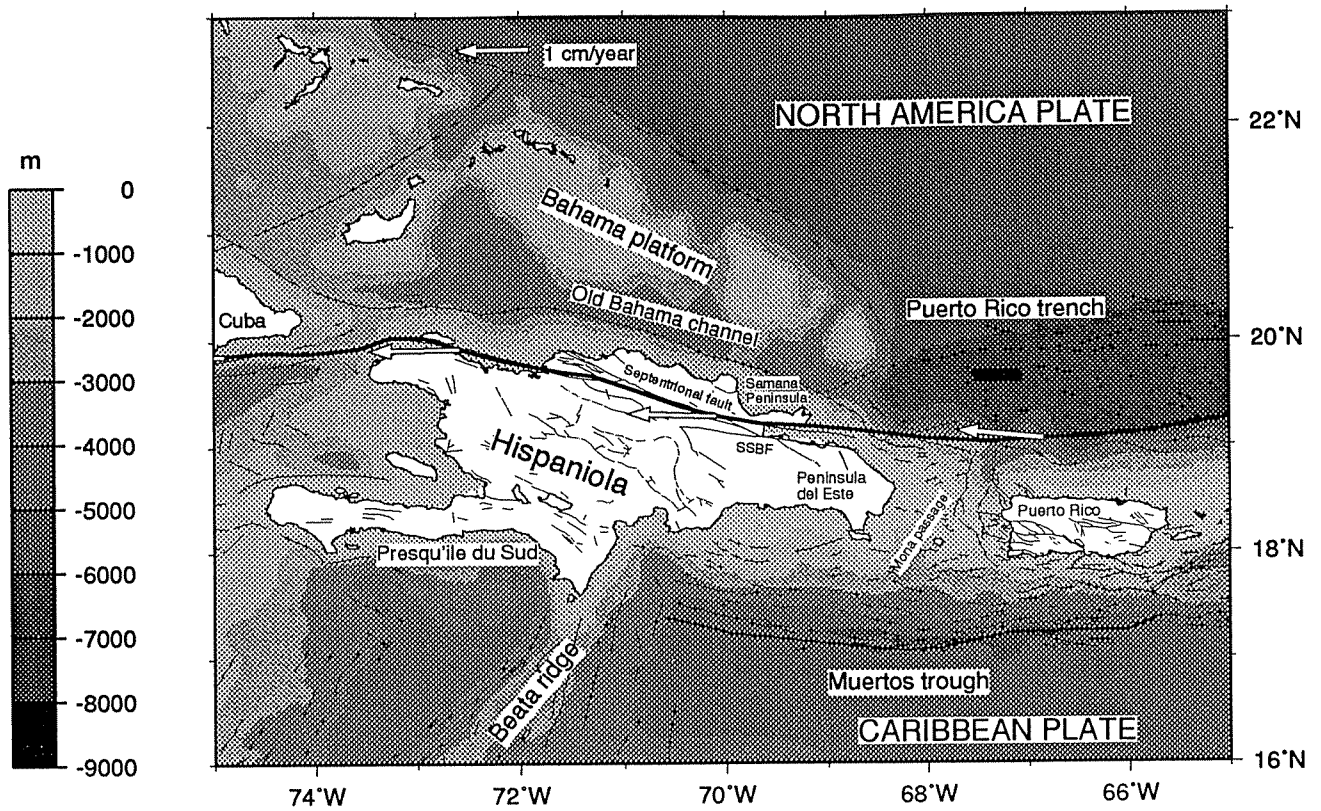

Figure 1a. Study region, Hispaniola and vicinity. Bathymetry (200 m and every kilometer thereafter) and faults from *Case and Holcombe,* [1980]. SSBF, South Samaná Bay Fault. Note location of Samaná Peninsula. Open arrows are NUVEL-1 NA-Ca velocity vectors.

It is surprising that this important earthquake series has eluded all study save routine location and magnitude estimation. In an effort to rectify this situation, we have taken a threefold approach to analyze the events and their tectonic significance. First, we relocated the main shock and aftershocks, and we compared our results to the distribution of recent (post-1963) seismicity of the region, and to the pattern of mapped faults and terranes. We constrained mechanisms for the main shock and three large magnitude aftershocks, and we analyzed nodal plane orientations in light of mapped faults to draw conclusions regarding the tectonic motions represented. We reevaluated the magnitude of the main shock and several large aftershocks. Finally, we comment briefly on the implications of our results for seismic hazard in eastern Hispaniola. As we discuss below, the event and its aftershocks are a complex mix of westward directed thrusting and WNW trending left-lateral strike-slip. It seems likely that these earthquakes represent the true long-term interplate motions between North America and the terranes in this portion of the plate boundary zone.

Tectonic Setting

Hispaniola lies within the complex North America-Caribbean plate boundary zone [*Molnar and Sykes,* 1969; *Jordan,* 1975; *Stein et al.*, 1988; *Lewis and Draper,* 1990; *McCann and Pennington,* 1990] between subducted North American oceanic lithosphere to the north and east [*Molnar and Sykes,* 1969; *Fischer and McCann,* 1984; *van der Hilst,* 1990; *Calais et al.*, 1992], and subducting [*Ladd et al.*, 1981; *Byrne et al.*, 1985] oceanic Caribbean lithosphere of the Venezuela Basin

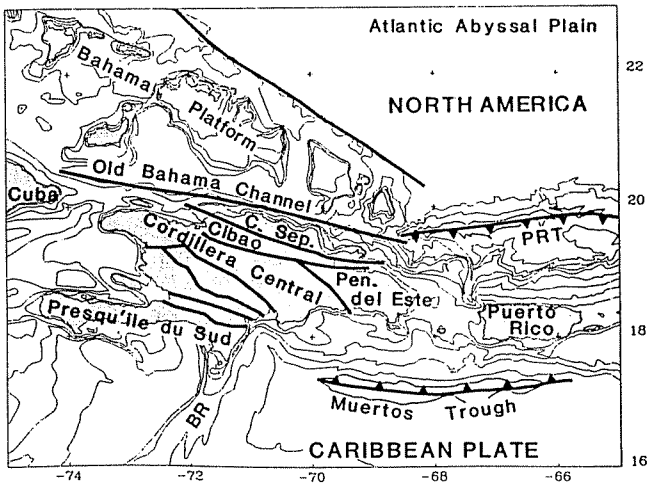

Figure 1b. Terranes and tectonic boundaries (heavy lines) discussed in text. C. Sep., Cordillera Septentrional; Cibao, Cibao Basin; C, Cuba; PRT, Puerto Rico Trench; BR, Beata Ridge. Heavy lines with teeth approximate surface projection of lithospheric subduction traces in Muertos Trough and Puerto Rico Trench.

to the south. There appears to be some question as to whether North America is actively subducting beneath the terranes of the plate boundary zone at the Puerto Rico Trench (Figure 1b) or is instead subducted but moving with purely strike-slip motions along the former subduction interface (see *Fischer and McCann* [1984] for discussion). Indeed, the Puerto Rico Trench may be the site of extension [*Talwani et al.*, 1959; *Jordan*, 1975; *Speed and Larue*, 1991] or convergence [*Molnar*, 1977; *Fischer and McCann*, 1984]. Nevertheless, the plate boundary zone in the vicinity of Hispaniola includes a strong component of left-lateral strike-slip motion [*Jordan*, 1975; *Sykes et al.*, 1982; *Mann et al.*, 1984; *Lewis and Draper*, 1990; *DeMets et al.*, 1990; *Calais et al.*, 1992] and may be the locus of a transition from subduction of oceanic North America beneath plate boundary terranes, to the east, to strike-slip relative motion between terranes in a wide strike-slip plate boundary, to the west.

A brief discussion of the terranes in and around Hispaniola is warranted to establish the positions of major tectonic boundaries in the vicinity of the 1946 earthquake series (Figure 1b). Between the Atlantic (Nares) Abyssal Plain, clearly part of the North American Plate [*Grow and Sheridan*, 1988], and the Venezuelan Basin region of the Caribbean Plate, south of the Muertos Trough, we consider several tectonostratigraphic units that comprise the wide (200 km) plate boundary zone. The northernmost unit, the Bahamas Platform [*Sheridan et al.*, 1988], is most likely underlain by Middle Jurassic Atlantic ocean basement and consists of Upper Jurassic to Cenozoic limestone reefs and marine sediments. South of the platform is the 3-km-deep Old Bahama Channel [*Lewis and Draper*, 1990], geomorphically the western extension of the Puerto Rico Trench (Figure 1b). This sediment-filled asymmetric basin terminates steeply at its south flank, adjacent to Hispaniola. Here, deepwater sediments are in north directed thrust imbricates [*Austin*, 1983] that perhaps mark the northernmost limit of plate boundary related deformation.

South of the channel, the northernmost terrane exposed on Hispaniola is a composite of fault-bounded metamorphic units, the Cordillera Septentrional [*Lewis and Draper*, 1990] and Samaná Peninsula rocks [*Joyce*, 1991]. The Samaná Peninsula, which lies just north of the epicenter of the August 4, 1946, main shock, includes a Late Cretaceous subduction complex that underwent Eocene metamorphism [*Joyce*, 1991]. The Cordillera Septentrional, adjacent to the Samaná Peninsula on the mainland, also includes subduction-related metamorphic and igneous units [*Lewis and Draper*, 1990]. Eocene-to-early Miocene turbidites unconformably overlie the metamorphic units and are in turn unconformably overlain by Miocene sediments and late Cenozoic reef complexes. Pervasive deformation of the sediments indicates that they have been involved in the North America-Caribbean plate boundary deformation since the middle or late Miocene. The uplift of the reef units demonstrates that this deformation is still active [*Horsfield*, 1975].

The Cordillera Septentrional and the Samaná Peninsula are bounded to the south by the Septentrional Fault Zone (Figures 1a and b). This zone consists of several strands of left-lateral strike-slip faults, including the South Samaná Bay Fault (SSBF), that cut across northern Hispaniola trending about N70°W [*Case and Holcombe*, 1980; *Mann et al.*, 1984; *Lewis and Draper*, 1990]. The magnitude of displacement on the fault zone is not well known because of the lack of correlatable rock units across the fault zone [*Lewis and Draper*, 1990].

South of the Septentrional Fault Zone (SFZ), we consider three tectonic units. The Cibao Basin, bounded on the north by the SFZ, contains thick (9 km [*Bowin*, 1960]), largely undeformed Miocene-Pliocene marine sediments. The basin's southern termination is a series of faults parallel to the SFZ that cross Hispaniola. To the east, the Cibao Basin terminates at the South Samaná Bay Fault (Figures 1a and b) [*Lewis and Draper*, 1990]. The basin formation and development were likely controlled by the tectonics of the fault zones. South of the eastern SSBF, in the Peninsula del Este, is another Cretaceous-Eocene subduction complex in which at least some of the rocks are isoclinally folded with southward vergence [*Lewis and Draper*, 1990]. The southernmost unit we consider is the Presqu'il du Sud terrane (Figure 1b) [*Maurrasse et al.*, 1979; *Lewis and Draper*, 1990] is interpreted as uplifted Caribbean crust of the Venezuela Basin [*Maurrasse et al.*, 1979].

The southern limit of the NA-Ca plate boundary zone lies south of the Peninsula del Este and Presqu'il du Sud terranes, offshore. Deformation of sediments observed through analysis of marine seismic reflection data [*Ladd et al.*, 1977; *Ladd and Watkins*, 1978; *Ladd et al.*, 1981] as well as earthquake focal mechanisms [*Byrne et al.*, 1985] have been interpreted as evidence for northward subduction of Caribbean lithosphere beneath Hispaniola at the Muertos Trough (Figure 1b). Thus Hispaniola may lie over and between two subducted oceanic lithospheres.

Event Relocations

We relocated the August 4, 1946, main shock, 61 aftershocks, and one foreshock (Figure 2 and electronic supplement Table A1[1]) using a generalized least squares iterative location routine that minimizes the difference between observed arrival times and those calculated based on a location estimate and the Jeffreys-Bullen Earth model [*Wysession et al.*, 1991; *Russo et al.*, 1992].

[1] An electronic supplement of this material may be obtained on a diskette or by anonymous FTP from KOSMOS.AGU.ORG. (LOGIN to AGU's FTP account using ANONYMOUS as the username and GUEST as the password. Go to the right directory by typing CD APEND. Type LS to see what files are available. Type GET and the name of the file to retrieve data file. Finally, type EXIT to leave the system.) (Paper 94JB02599, The 1946 Hispaniola earthquakes and the tectonics of the North America-Caribbean plate boundary zone, northeastern Hispaniola, R. M. Russo and A. Villaseñor). Diskette may be ordered from American Geophysical Union, 2000 Florida Avenue, N. W., Washington, DC 20009; $15.00. Payment must accompany order.

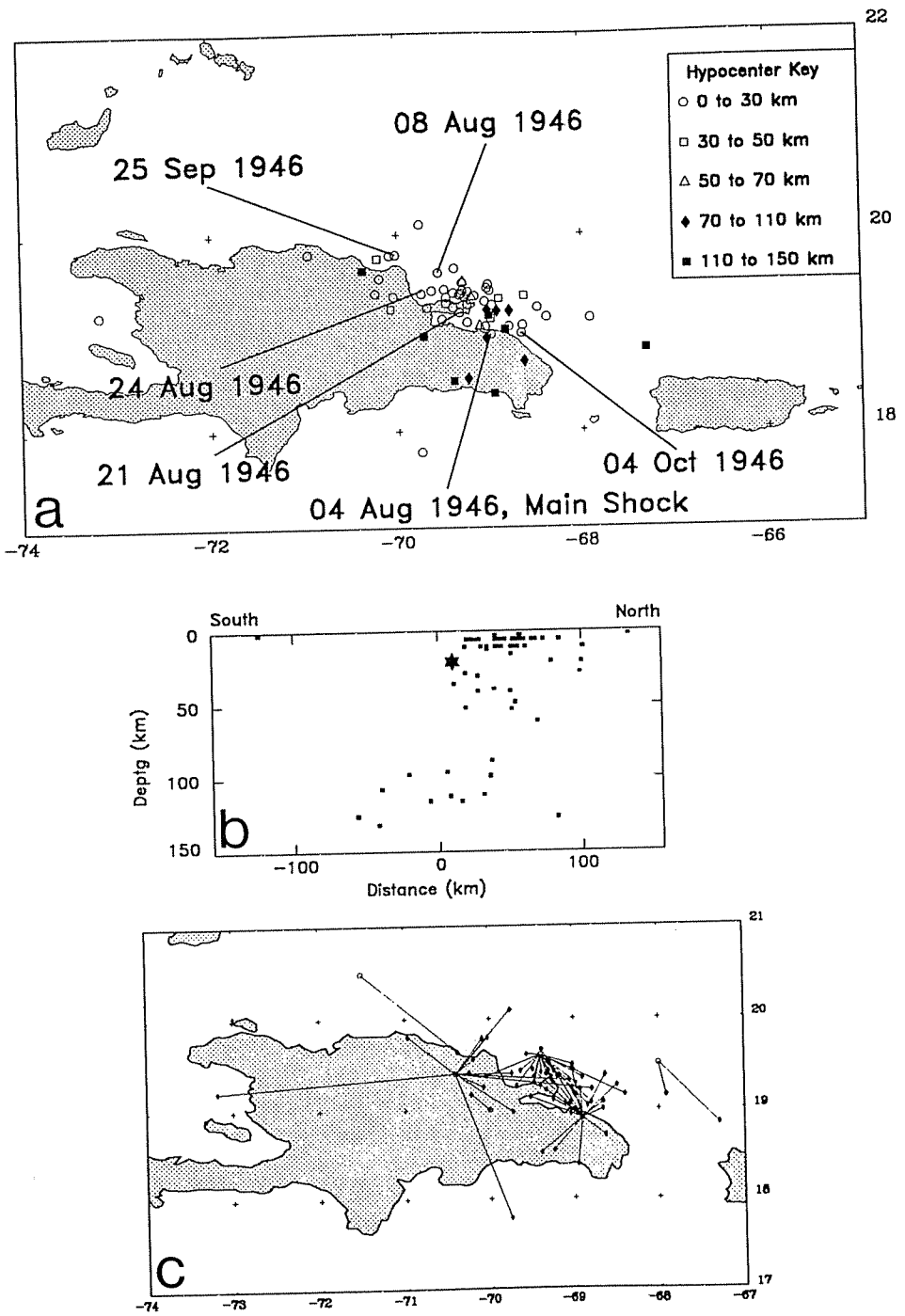

Figure 2. (a) Relocated earthquakes of the 1946 series. Main shock and larger magnitude aftershocks discussed in text labeled. Depths of events indicated by symbols in key. (b) Vertical projection onto N-S plane of all the 1946 events. Main shock indicated by star. (c) Relocation vectors of events. Open symbols are ISS original locations; solid symbols our relocations.

We used arrival times published in the International Seismological Summary (ISS) bulletins for the years 1946 and 1947. In almost all cases, we were able to locate the events to a precision such that the summed residual, or difference between observed and calculated arrival times, was less than 3.0 s. Whenever possible, we allowed the hypocentral depth to vary during this procedure; in cases where the depth would not float we fixed it at an approximate depth determined by performing relocations for a range of fixed depths using all available data and choosing the depth which yielded the minimum travel time residual for the actual relocation. Most often, this fixed depth was 5 km, 2 km, or 10 km for these events (Table A1). However, as we discuss below, waveform modeling of the four events with mechanisms reveals that for these events the relocation depths are consistently too shallow by some 10 to 20 km. On this basis for these four events, we refixed depths at the

deeper value and reinverted the travel times; these new locations were virtually indistinguishable from the locations with shallower fixed depths, and so we maintained the original epicentral relocations.

The relocations are shown in Figure 2a. We locate the main shock, August 4, 1946, on the north coast of the Peninsula del Este (Figure 1b). The aftershock series trends WNW from the main shock, is centered on the Samaná Peninsula (Figure 1a), and extends approximately 250 km. The main shock and the majority of the aftershocks occurred at shallow depths. However, several aftershocks apparently occurred deeper than 70 km, and the deepest event in the series attained 130 km depth. The intermediate depth ($h > 70$ km) aftershocks lie in the southeast quadrant of the complete aftershock series, with two widely separated exceptions. We note that the main shock (August 4, 1946) is the southernmost of the shallow events of the aftershock series (excluding two outlier events, one far to the south of the series in the Muertos Trough, and a second west of Haiti).

Projected vertically onto a north-south section (Figure 2b), the aftershock series comprises a nearly 75 km wide zone of shallow events, a group of events at depths of 30 to 60 km, and a group of intermediate depth events between 75 and 130 km. Overall, the distribution resembles a poorly defined south or SSW dipping Benioff zone. We note that the relocations are based almost exclusively on teleseismic stations, and we were not able to examine seismograms for depth phase information for any of the deeper events.

A comparison of the relocations to the original ISS locations is shown in Figure 2c. The ISS located all the events in the aftershock series to six surface epicenters. The clear spread of the relocations from the ISS locations illustrates the inadequacy of the original locations. The good azimuthal spread of the relocation vectors demonstrates the lack of station distribution bias in the relocations. The relocations are largely consistent with the observations of surface deformation by *Lynch and Bodle* [1948], made on site shortly after the 1946 events.

Focal Mechanisms

Polarities and Amplitude Ratios

We determined new focal mechanisms for the main shock and three large magnitude aftershocks. We did this using two independent methods. In the first method, we used a combination of first motion picks read by us on available seismograms, reported ISS first motion polarities, and constraints from *SV* and *SH* polarities and *SV/P*, *SV/SH* amplitude ratios, also observed by us on available seismograms. We also modeled waveforms of these events. We obtained seismograms from World Data Center-A for Solid Earth Geophysics in Denver and from individual stations in North America and Europe. The recording seismometers included both mechanical and early electromagnetic seismographs (Table 1).

We derived focal mechanisms by performing a grid search of the focal sphere for solutions consistent with the observed first motions, *S* polarities, and amplitude ratios [*Kisslinger,* 1980; *Snoke et al.,* 1984]. The method provides a good estimate of the range of solutions compatible with the data set. We discuss the individual events and data used to constrain mechanisms below. The station information and focal mechanism parameters are detailed in Tables 1 and 2. The mechanisms and data plotted on lower focal hemispheres are shown in Figure 3.

August 4, 1946. For the main shock we used 12 *P* polarities, two *SV*, three *SH* polarities, and eight amplitude ratios. One nodal plane, striking NW and dipping nearly 70°NE, is reasonably constrained from the *P* first motion data (Figure 3a). The majority of these are compressional arrivals at North and South American stations; we observed a dilatational arrival at Weston and the ISS report a dilatational arrival at Harvard. The ISS reports mixed polarities for European stations. We examined seismograms from stations in Spain (EBR and FBR) and confirmed that arrivals were emergent. These polarity ambiguities may reflect proximity to the nodal plane of rays taking off to these stations, and indeed, our final focal mechanism confirms this geometry for many European stations. The focal mechanism must correspond to thrusting, but the second nodal plane is otherwise undetermined by the first motion data alone, necessitating recourse to constraints from *S* wave polarities and to amplitude ratios. The *SV* waves at Fabra (FBR, Barcelona, Spain) and at Ottawa (OTT, Canada) are both polarized such that the *SV* first motion is away from the source, or positive in *Kanamori and Stewart*'s [1976] convention for *S* polarities. We also determined *SH* polarities at Huancayo (HUA, Peru), College (CMO, Fairbanks, Alaska), and Salt Lake City (SLC, Utah). At all three sites, the *SH* polarity is negative. We supplemented polarity information with *SV/P* amplitude ratios at La Paz (LPZ, Bolivia) and with *SV/SH* ratios at Tucson (TUO, Arizona), HUA, Sitka (SIT, Alaska), SLC, CMO, FBR, and Honolulu (HON, Hawaii). In all cases, we corrected the amplitude ratios for free-surface interaction based on theoretical *S* takeoff angles. The resulting mechanism is a thrust event with a significant component of strike-slip motion (Table 2 and Figure 3a). The second nodal plane strikes N-S and dips shallowly west. The data constrain the mechanism very well: the range of allowed nodal plane parameters is ± 3°for both strike and dip, and ± 5°for the slip angle.

August 8, 1946. The data available for this event were nine *P* (six from the ISS), one *SV*, and three *SH* polarities, and 10 amplitude ratios. The *P* first motion data indicate a mechanism different from the main shock for this earthquake: stations in North America and Europe now lie in a dilatational quadrant, and South American stations (HUA and LPZ) record compressional first arrivals. The first motion data indi-

Table 1. Station Parameters

Station	Code	Latitude °N	Longitude °E	Instruments	Components
Bozeman, Montana	BZM	45.67	-111.03	McComb-Romberg	N-S, E-W
College, Alaska	COL	64.90	-147.78	McComb-Romberg	N-S, E-W
Columbia, South Carolina	CSC	34.00	-81.03	McComb-Romberg	N-S, E-W
Roquetes, Spain	EBR	40.82	0.48	Ebro-vertical, Mainka	SPN, N-S, E-W
Barcelona, Spain	FBR	41.40	2.12	Mainka	N-S, E-W
Honolulu, Hawaii	HON	21.32	-158.01	Milne-Shaw	N-S, E-W
Huancayo, Peru	HUA	-12.03	-75.32	Benioff	Z, N-S, E-W
La Plata, Argentina	LPA	-34.90	-57.92	Mainka	N-S, E-W
La Paz, Bolivia	LPZ	-16.48	-68.12	Galitzin-Willip	Z, N-S, E-W
Mount Hamilton, California	MHC	37.33	-121.63	Wood-Anderson	N-S, E-W
Ottawa, Canada	OTT	45.38	-75.70	Benioff, Milne-Shaw	SPZ, LPZ, N-S, E-W
Pasadena, California	PAS	34.13	-118.17	Benioff	SPZ, LPZ
Salt Lake City, Utah	SLC	40.75	-111.83	McComb-Romberg	N-S, E-W
Sitka, Alaska	SIT	57.05	-135.32	Wenner	N-S, E-W
San Juan, Puerto Rico	SJP	18.38	-66.12	Wenner	N-S, E-W
Tucson, Arizona	TUO	32.23	-110.83	Benioff, Wood-Anderson	SPZ, LPZ, N-S, E-W
Weston, Massachusetts	WES	42.38	-71.31	Benioff	3 SP, 3 LP

Z, vertical; SP, short-period; LP, long-period; SPN, SP N-S.

cate that one nodal plane must dip rather steeply but otherwise provide little constraint on the mechanism. We used the *SV* polarity from Weston (WES, Massachusetts; back to source, or negative) and *SH* polarities at WES, TUO, and OTT. The *SH* polarities are all positive. *SV/P* amplitude ratios from WES and Pasadena (PAS, California), and *SV/SH* ratios from WES, HUA, SIT, SLC, La Plata (LPA, Argentina), TUO, CMO, and OTT complemented the polarity data. The resulting focal mechanism (Figure 3b) is well constrained, with a moderately dipping nodal plane striking WNW, and a near vertical plane striking NNE. The mechanism thus corresponds to almost pure strike-slip, left-lateral on the WNW striking plane, and dextral on the other plane. We note that although the mechanism is quite different from that of the main shock, they both have NW striking nodal planes.

August 21, 1946. The data set for this earthquake included 12 *P*, two *SV*, two *SH* polarities, and four *SV/SH* amplitude ratios. First motion *P* dilatations were observed at South American and European stations. Stations in North America lie in a compressional quadrant. Again, one nodal plane is constrained to dip steeply. We determined *SV* polarities at HUA (negative) and Bozeman (BOZ, Montana; negative), and *SH* polarities at Columbia (CSC, South Carolina; positive) and at SIT (positive). The amplitude ratios are from CSC, HUA, BOZ, and SIT. The solutions compatible with the data include strike-slip and normal faulting. The range of nodal plane parameters is ± 10°in strike, ± 5°in dip, and ± 10°slip. Our preferred mechanism (Figure 3c) is left-lateral strike-slip on a NW striking, SW dipping plane, or dextral strike-slip on a near vertical NE striking plane. We again note the presence of a NW striking nodal plane.

August 24, 1946. We could not constrain the mechanism of this aftershock given the paucity of data available to us: eight *P* and one *SH* polarities and one *SV/SH* amplitude ratio at the near station, SJP. However, the data indicate that the earthquake has predominantly a thrust mechanism (Figure 3d), and the available data are all consistent with the mechanism of the main shock, August 4, 1946.

September 25, 1946. We used six *P*, one *SV*, and

Table 2. Focal Mechanism Parameters

Date	Latitude °N	Longitude °W	Depth, km	Magnitude	Strike	Dip	Slip	Moment, N m
Aug. 4, 1946	18.99	68.99	20[a]	7.8	303	62	74	
Aug. 8, 1946	19.61	69.56	20[a]	7.3	315	25	-10	
Aug. 21, 1946	19.21	69.33	12[a]	6.2	137	62	-11	1.98×10^{18}
Aug. 24, 1946	19.43	69.63	5	—	thrust event			
Sep. 25, 1946	19.80	70.02	20	5.4	thrust event			
Oct. 4, 1946	19.00	68.66	35[a]	6.1	87	33	64	8.76×10^{17}

[a]Depth from waveform modeling.

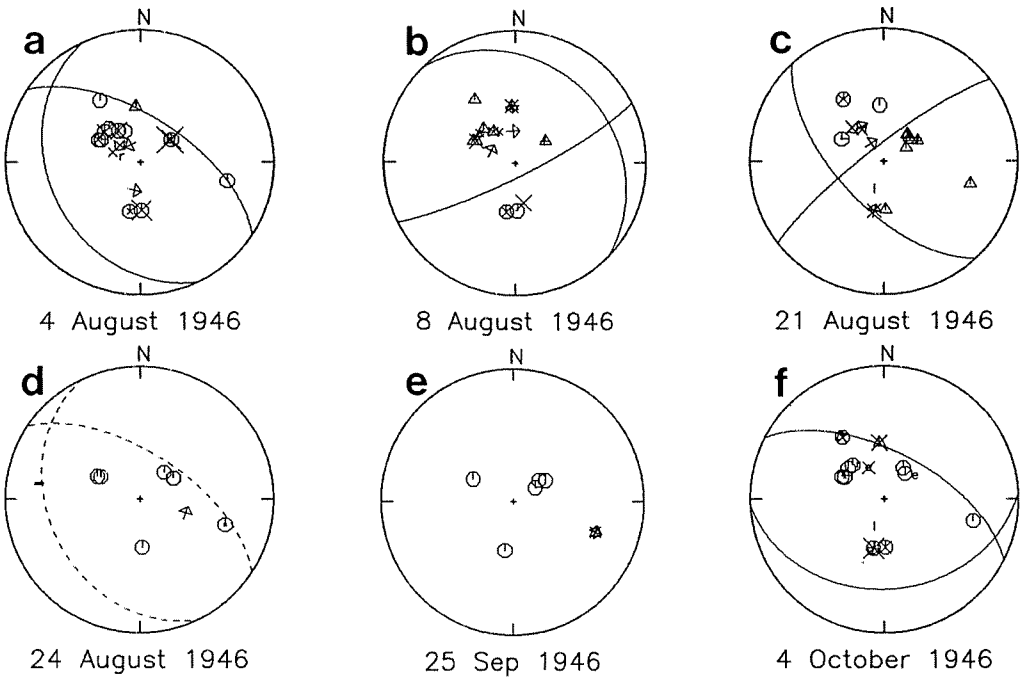

Figure 3. Focal mechanisms and data plotted on lower focal hemisphere. Hexagons are compressional P first motions, triangles are dilatations. Crosses indicate amplitude ratio constraint. Arrows show S polarities. Note nodal planes of main shock projected on data for August 24 event (Figure 3d).

one SH polarities, and one SV/SH amplitude ratio in an unsuccessful attempt to constrain the mechanism of this aftershock. As with the August 24, 1946 event, the first motion data indicate that the event was predominantly a thrust (Figure 3e).

October 4, 1946. A data set of 14 P and two SV polarities, and three SV/P and four SV/SH amplitude ratios yielded a very well constrained thrust event. First motion polarities were identical to those of the main shock, and where there was data overlap, also with the August 24, 1946 event. We determined SV polarities at HUA and CSC (both positive). SV/P ratios are from WES, LPB, and PAS; SV/SH ratios are from WES, HUA, CSC, and CMO. Again, one of the nodal planes, which is very well constrained, strikes approximately N60°W (Figure 3f).

Waveform Modeling

The method that we used above to constrain focal mechanisms is dependent upon a clear identification of phases for which amplitude ratios are measured. For shallow earthquakes at teleseismic distance it may be difficult to separate direct arrivals from surface reflections (pP, etc.). In order to demonstrate that the mechanisms are not adversely affected by mixing of direct and reflected phases, we performed waveform modeling on the four earthquakes described above. Additionally, body wave waveforms are very sensitive to focal depth and to the orientation of the double couple. Therefore waveform modeling is useful for checking the calculated focal depth and the reliability of the fault plane solution. Normally, depth uncertainties are reduced an order of magnitude with respect to teleseismic locations such as ours. This reduction is even greater when short-period data are used. In using this method, it is possible to match true waveform shapes and amplitudes or solely the waveform shape. If both shape and amplitude are matched, an estimation of the seismic moment can also be obtained.

We use a method involving both forward and inverse modeling of P and SH waveforms [*Nabalek*, 1984; *McCaffrey et al.*, 1991; *Bjarnasson and Einarsson*, 1991] based on techniques developed originally by *Helmberger* [1974] and *Langston and Helmberger* [1975]. The seismic source is modeled as a double-couple point source parameterized by the strike and dip of the fault plane and slip vector within the plane, the centroid depth of the event, and the source-time function of the rupture. The source-time function is represented by a set of overlapping isosceles triangles [*Nabalek*, 1984] forming a smooth representation of the source-time function. Source structure is assumed to be a half-space with a P wave velocity of 6.5 km/s, S wave velocity of 3.7 km/s, and a density of 2.8 g/cm^3. Receiver structures are assumed to be half-spaces. The data used are from both mechanical and electromagnetic seismometers, and the instrument responses are modeled by ideal pole-zero representation and galvanometer and damping ratios, respectively.

The results of the waveform modeling are shown in Figures 4 and 5. First, we did some trials to obtain an estimate of the shape and duration of the source time

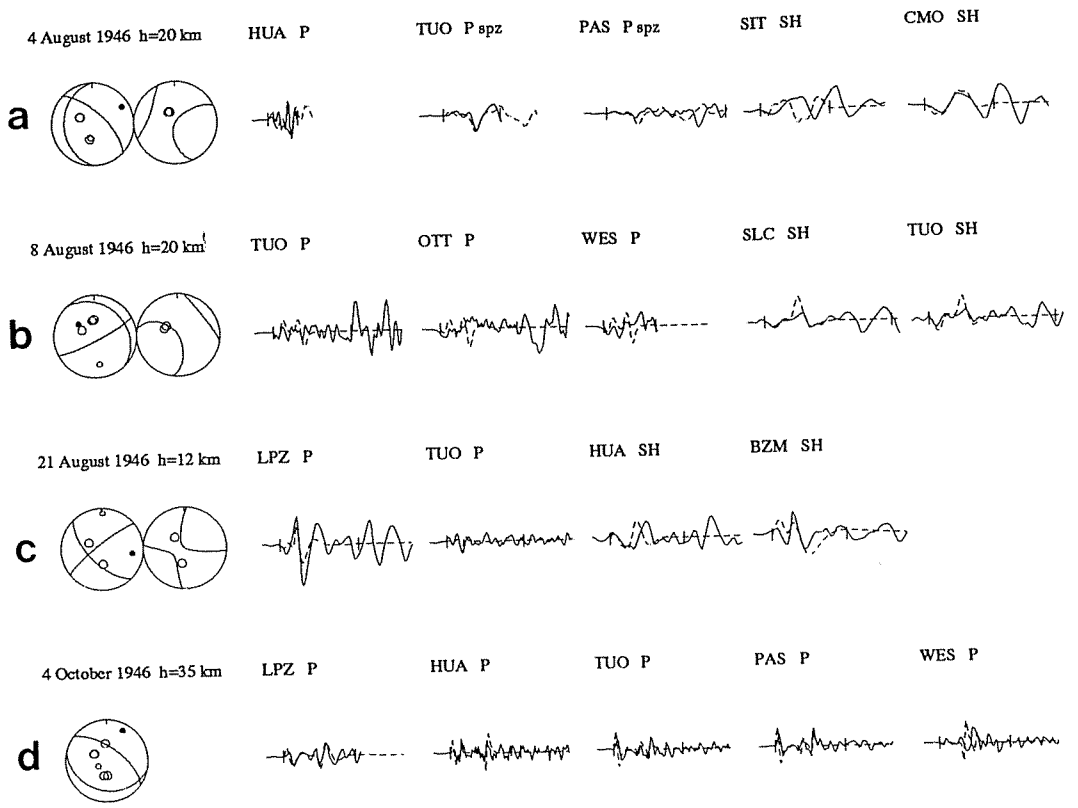

Figure 4. Waveform analysis to constrain depths of the main shock and three large-magnitude aftershocks. Lower hemisphere focal mechanisms shown, solid dot is P axis, open dot is T axis; open circles are positions of takeoff rays to stations. Both P (left beachball) and, where modeled, SH (right beachball) shown. Dashed waveform traces are synthetics, solid traces are data. (a) August 4 waveform matches, 20 km focal depth. Note good fit of TUO short period P (increases resolution) and CMO SH. Polarities of all phases are matched; note apparent timing error at SIT. (b) August 8 waveform matches, 20 km focal depth. Polarities are matched, but P waveform fits are not as good as for the main shock. SH waveforms at SLC and TUO are better fit, however, and are less sensitive to errors in the source-time function than the P waves. (c) August 21 waveform fits at 12 km depth. Again, polarities are matched, and observed and synthetic waveforms are very similar for all stations. (d) Waveform matches for October 4 event at 35 km depth. Polarities and waveforms match quite well for all stations.

function (STF). For the August 21 and October 4 events a single triangular source of 2 s duration was sufficient to represent the observed seismograms. For the August 4 and 8 events, as expected, the source time function is longer and more complicated. The main shock (Figure 5) has two subevents and a 10 s length. The Aug. 8 event is well-modeled by a triangular STF of 4 s. For both events we were unable to find a satisfactory waveform fit with simple and short STF's.

In order to obtain an improved estimate of the event depths, we forward modeled waveforms at discrete fixed values of the focal depth, using the focal mechanisms we had constrained from the first motion/amplitude ratios (Figure 4). A simple comparison of observed and synthetic seismograms constrains the focal depth and its uncertainty. For the August 21 and October 4 events we obtained very good matches between observed and synthetic waveforms. We were able to constrain the depths of these events at 12 km and 35 km, respectively (Figure 4). For the two larger magnitude events (August 4 and 8) the waveform matches were somewhat poorer, probably because of complex ruptures and the effects of attempting to match a synthetic based on a point source assumption to finite source events. We adjusted the strike of the August 8 event (from 301 to 315°to better fit the waveforms. In any case, the shapes and polarities of P and SH waveforms are satisfied for focal depths of 20 km for both of these two events (Figure 4). We note that the waveform-derived depths maintain the relative depths we found using the teleseismic relocations: the deepest event in both cases is the October 4 earthquake, and the shallowest is the August 21 aftershock; and the main shock and the August 8 shock were constrained to the same depth (20 km waveform, 5 km relocation). In all cases we can clearly identify the surface reflected phases, pP and pSH, and they are well separated from the initial direct P and direct SH arrivals. Thus we are assured that we did not mix direct and surface-reflected energy when we measured the amplitude ratios used to constrain the focal mechanisms. Additionally, the good waveform matches between the synthetics derived from these mechanisms and the data

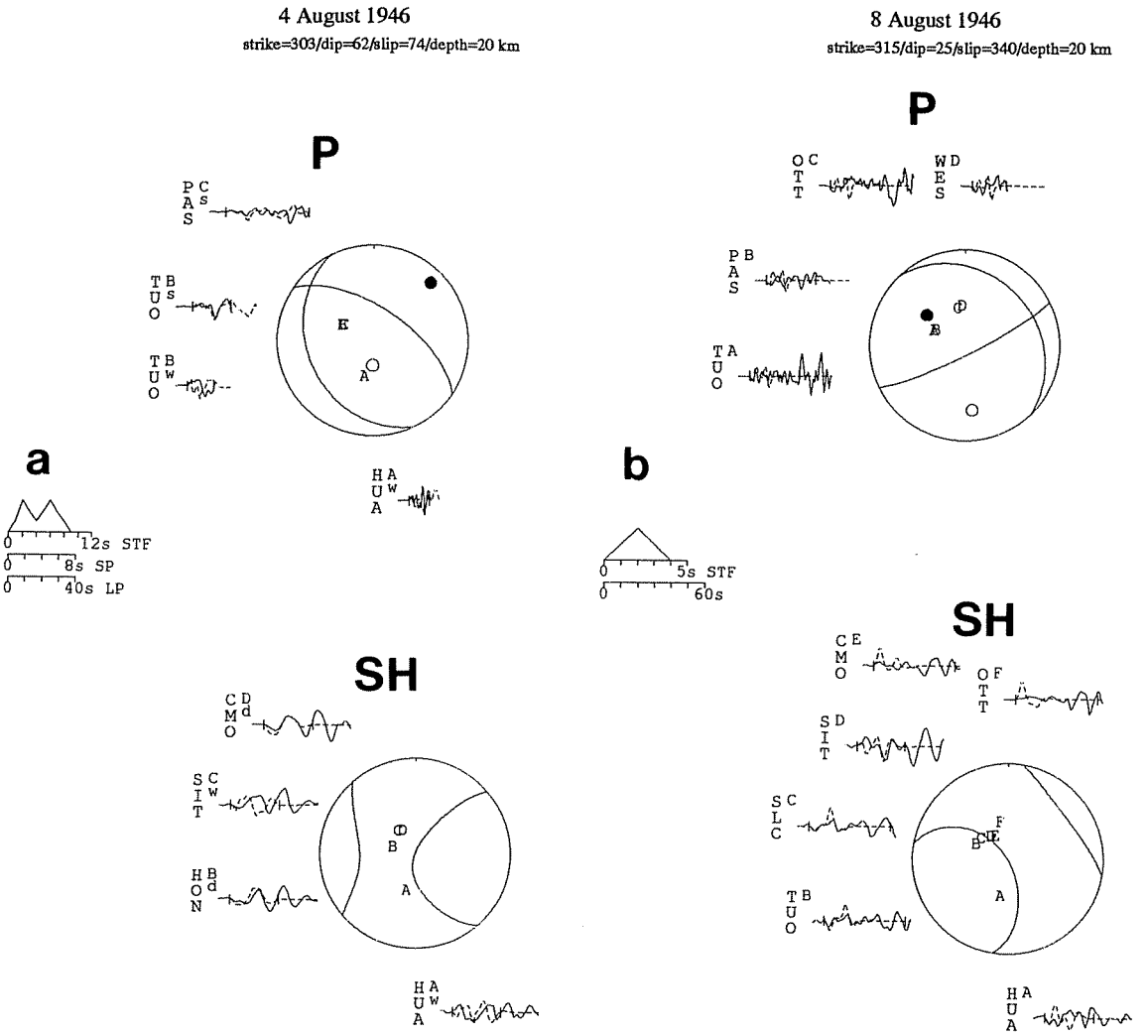

Figure 5. Waveform fitting to confirm focal mechanisms. Lower hemispheres shown, solid dot is P axis, open dot is T axis. Letters within beachballs indicate takeoff angles to various stations. Source-time functions (STF) used also shown at center left. (a) August 4, 1946, Main shock. (top) P waves, (bottom) SH waves. Note inclusion of short period P wave data, labeled with a small s beneath letter code. Waveforms are well fit for PAS long-period P (A), TUO short-period P (B), HUA long-period P (A), CMO long-period SH (D), and HON long-period SH. Note apparent timing error at SIT (C). Waveform amplitudes not matched, and hence seismic moment not estimated. (b) Same as Figure 5a but for August 8 event. Note good waveform fitting for TUO lp P waves (A) and for SLC and TUO lp SH waves. Poor matches of SIT and CMO SH may be due to proximity of nodal surface. (c) Waveform matches for August 21 event. P wave data well fit for both stations. SH waves fit best at CSC. Amplitude scale is in microns and yields a seismic moment of 1.98 x 10^{18} N m. (d) Waveforms for October 4 event. All P wave data are matched very well. SH is well fit at SLC and reasonably well at HUA. Seismic moment is estimated at 8.76 x 10^{17} N m.

provide direct confirmation that the mechanisms correctly fit the available data.

For the two later events we were able to fix the focal mechanisms and invert the waveforms for focal depth and seismic moment. The centroid depths obtained in the inversions are almost identical to those obtained using forward modeling. Inversion yielded a seismic moment of (Figure 5 and Table 2) 1.98 x 10^{18} N m for the August 21 earthquake, and 8.76 x 10^{17} N m for the 4 October event. These values are consistent with the magnitudes we estimate for the events (see below).

Event Magnitudes

We determined M_S magnitudes for eight of the earthquakes in the series (Table 3), including the main shock and the larger aftershocks for which we constrained mechanisms. Previously, magnitude estimates had been available for only three of the events [*Gutenberg and Richter,* 1954; *Abe,* 1981]: the main shock August 4 (8.1) and the August 8 (7.6), and October 4 (7.0) events. Gutenberg and Richter did not detail their method of determining magnitudes, however, and there is some

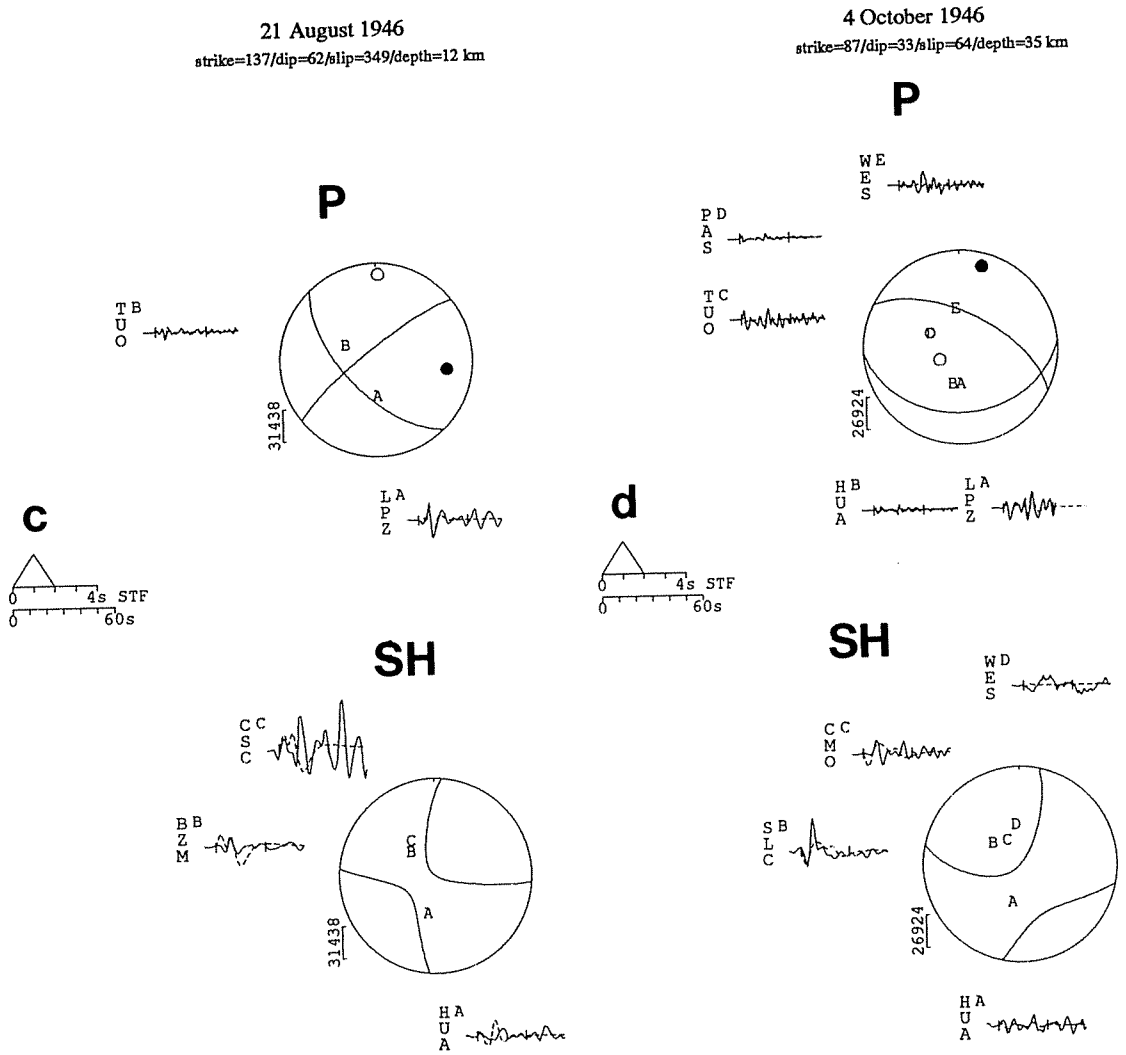

Figure 5. (continued)

question regarding comparing their magnitudes to those routinely calculated in the modern era. *Geller and Kanamori* [1977] and *Abe* [1981] found that magnitudes in the Gutenberg and Richter catalog (hereafter denoted M_{GR}) for shallow earthquakes ($h < 40$ km) are equivalent to modern M_S if an additive factor is included:

$$M_S = logA + 1.656log\Delta + 1.818 \qquad (1)$$

where Δ is the epicentral distance in degrees and A is the combined (vectorial sum) horizontal amplitude in microns of the maximum displacement of 20-s period surface waves. *Abe* [1981], in order to obtain a uniform magnitude catalog, recalculated the M_S magnitudes for these three earthquakes. We include both Abe's and Gutenberg and Richter's results in Table 3.

We used the Prague formula [*Vanek et al.*, 1962] to redetermine M_S magnitudes of the eight events:

$$M_S = log(\frac{A}{T})_{max} + 1.66log\Delta + 3.3 \qquad (2)$$

Table 3. Magnitudes

Date	Origin Time, UT	Latitude °N	Longitude °W	Depth, km	M_{GR}	M_S [*Abe*, 1981]	M_S (This Study)
Aug. 4, 1946	1751:05.0	18.99	68.99	20	8.1	8.0	7.8
Aug. 4, 1946	2053:31.1	19.41	70.24	5	—	—	5.1
Aug. 8, 1946	1328:30.3	19.61	69.56	20	7.6	7.6	7.3
Aug. 9, 1946	0825:40.5	19.43	69.30	5	—	—	5.3
Aug. 9, 1946	2006:38.3	19.26	68.49	2	—	—	5.6
Aug. 21, 1946	1917:40.8	19.21	69.33	12	—	—	6.2
Sep. 25, 1946	1005:43.0	19.80	70.02	20	—	—	5.4
Oct. 4, 1946	1445:26.5	19.00	68.66	35	7.0	6.4	6.1

where A is the vertical or resultant horizontal amplitude, T is the mean period and Δ is the epicentral distance in degrees. For shallow earthquakes our magnitudes are directly comparable to Abe's M_S measurements and to the M_{GR} estimates, except for the term 0.18. For the main shock, we calculate $M_S = 7.8$, and the smallest magnitude we determine is 5.1 for the most prominent aftershock on August 4, 1946. For the three largest earthquakes, our magnitudes are systematically less than those obtained by *Gutenberg and Richter* [1954] and by *Abe* [1981], even taking into account the additive factor mentioned above. It is not apparent why this is so.

Discussion

Event Relocations and Faults

We first examine the distribution of the 1946 earthquake series and its relationship to the known faults and tectonic boundaries we discuss above. As is clear in Figure 6, the long axis of the aftershock series, trending approximately WNW, is parallel to the principal faults and tectonic boundaries in northeastern Hispaniola. In particular, the long axis of the aftershock trend is approximately parallel to the Septentrional and South Samaná Bay Faults, although the centroid of the aftershock series lies north of these faults. The main shock most likely occurred several kilometers beneath the mapped trace of the South Samaná Bay Fault (Figures 1 and 6), although as we discuss below, the strike of our preferred nodal plane is different from the strike of the mapped fault, precluding definite association of the main shock and the South Samaná Bay Fault. The area of the shallow aftershocks is quite large, approximately 250 km by 75 km; we suggest therefore that the motions represented by the 1946 series are distributed over several faults or splays within the plate boundary zone. Unfortunately, the majority of these shallow events occurred in a region north of the Samaná Peninsula that is apparently devoid of mapped faults, however.

In order to place the relocated 1946 earthquake series in a tectonic context, we show recent (1963-1992) earthquakes recorded by 20 seismometers (to ensure some measure of hypocentral accuracy) in Figure 7. The recent shallow seismicity falls into two linear zones (Figure 7a), a northern strand 50-75 km wide of somewhat patchy character that between 69°W and 65°W trends E-W and is centered on 19°N; from 69°W to 71°W the northern strand trends more WNW, roughly parallel to the northeast coast of Hispaniola; west of 71°W, although there is some indication that the shallow seismicity again trends E-W, the number of events is too few to allow definite comment. The southern linear zone of shallow seismicity also trends E-W and is similarly 50-75 km wide. This strand follows the south coast of

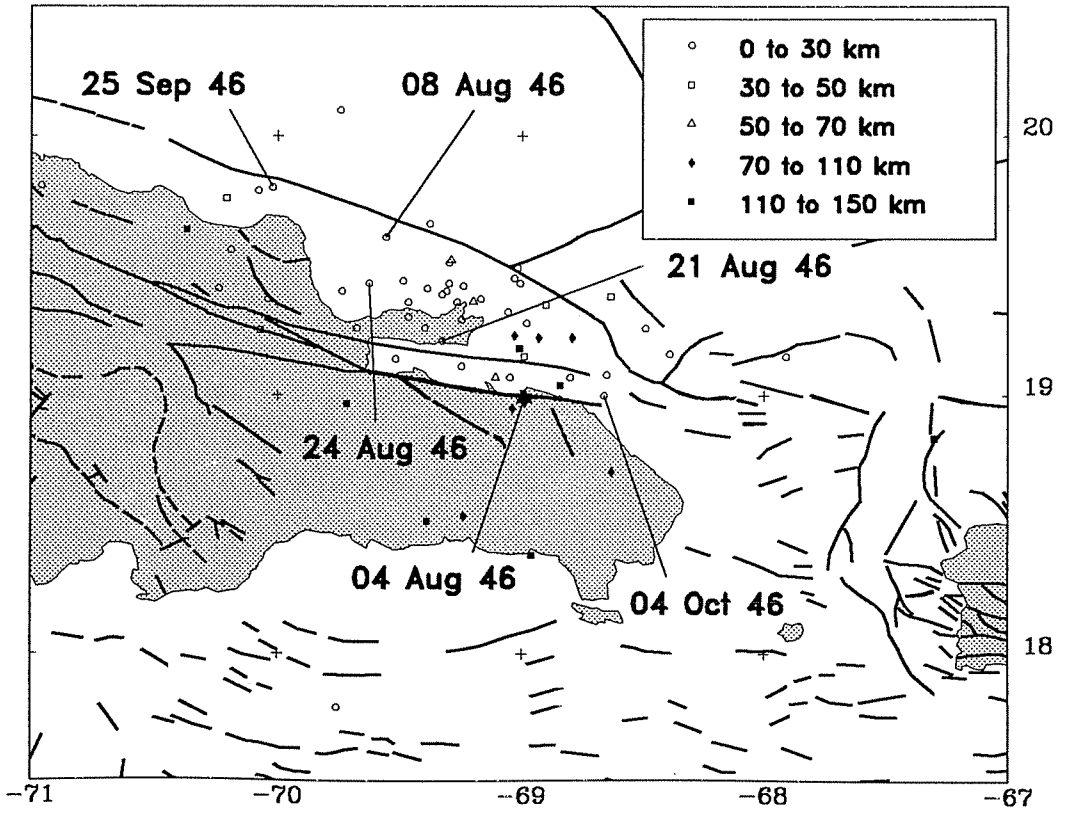

Figure 6. Event relocations superposed on mapped faults from *Case and Holcombe* [1980]. Note long axis of aftershock series, trending WNW, is approximately parallel to faults, especially Septentrional Fault Zone.

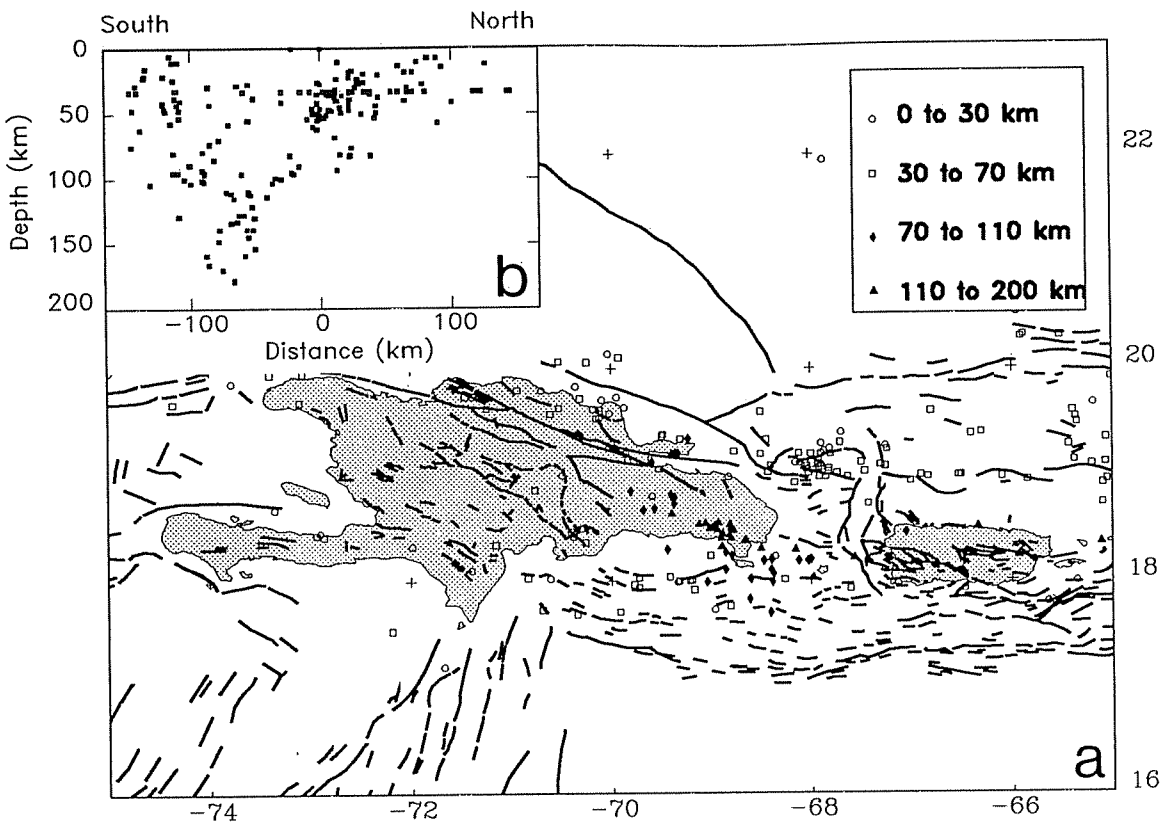

Figure 7. (a) Locations of recent (1963-1992) earthquakes located by the NEIC. Only events recorded by 20 or more stations shown. (b) vertical projection of events on map onto N-S plane.

Puerto Rico and continues west centered on 18°N to the eastern Presqu'il du Sud region of Haiti, where it too becomes difficult to discern due to lack of events. The location and trend of the 1946 series are clearly compatible with their inclusion in the northern strand of shallow events described above (compare Figures 6 and 7). We note, however, that the 1946 earthquakes occurred in a region where few recent shallow earthquakes have been detected. We believe that the stress release associated with the 1946 events was great enough to result in reduced seismicity in the vicinity of the Samaná Peninsula to this day.

The intermediate depth ($h > 70$ km) aftershocks, as mentioned above, appear to form an ill-defined south or SSW dipping slab. It is not clear whether these events occurred within a slab and indicate active subduction; or if they occurred at a strike-slip interface between subducted but no longer sinking lithosphere and overlying asthenosphere moving in the plate boundary zone. The more recent seismicity in cross section (Figure 7b) presents a complex triangular pattern of hypocenters with a steeply dipping southern limb and a more moderately dipping northern limb. It is possible that this pattern indicates the presence of two slabs, one dipping steeply north beneath the Muertos Trough [*Byrne et al.*, 1985] and a second dipping shallowly south.

Focal Mechanisms and Tectonics

The four focal mechanisms for the larger magnitude 1946 events differ in nodal plane orientation and slip directions (Figure 8). However, each mechanism has a NW striking nodal plane that is approximately parallel to the long axis of the aftershock trend and to the strikes of the principal regional faults. Therefore we choose these planes as fault planes. The dip of these fault planes to both northeast (main shock, August 8, and October 4) and southwest (August 21) is consistent with our interpretation that the width of the aftershock zone reflects displacements on several faults or splays. The two southeastern events, the main shock and the October 4 event, are both predominantly thrusts on the NW striking planes, whereas the two northwestern events have nearly pure left-lateral strike-slip on their NW striking planes. The main shock slip vector in the NW striking plane trends due west, the slip vector of the October 4 thrust trends SSW, and the slip vectors for the two strike-slip events are as defined. The principal axes of the four events are not systematic. The mechanisms and slip vectors are consistent with westward motion of the Cordillera Septentrional and Samaná Peninsula terrane relative to the remainder of Hispaniola. We interpret the due-west trend of the main shock slip vector on a NE dipping NW striking fault plane as the result of this westward motion of the terrane as it encounters a restraining bend in the otherwise predominantly left-lateral strike-slip NA-Ca plate boundary zone (Figure 9a). The existence of a restraining bend in eastern Hispaniola has been previously noted [*Mann et al.*, 1984; *Calais et al.*, 1992]. The thrusting represented by the main shock, in the SE

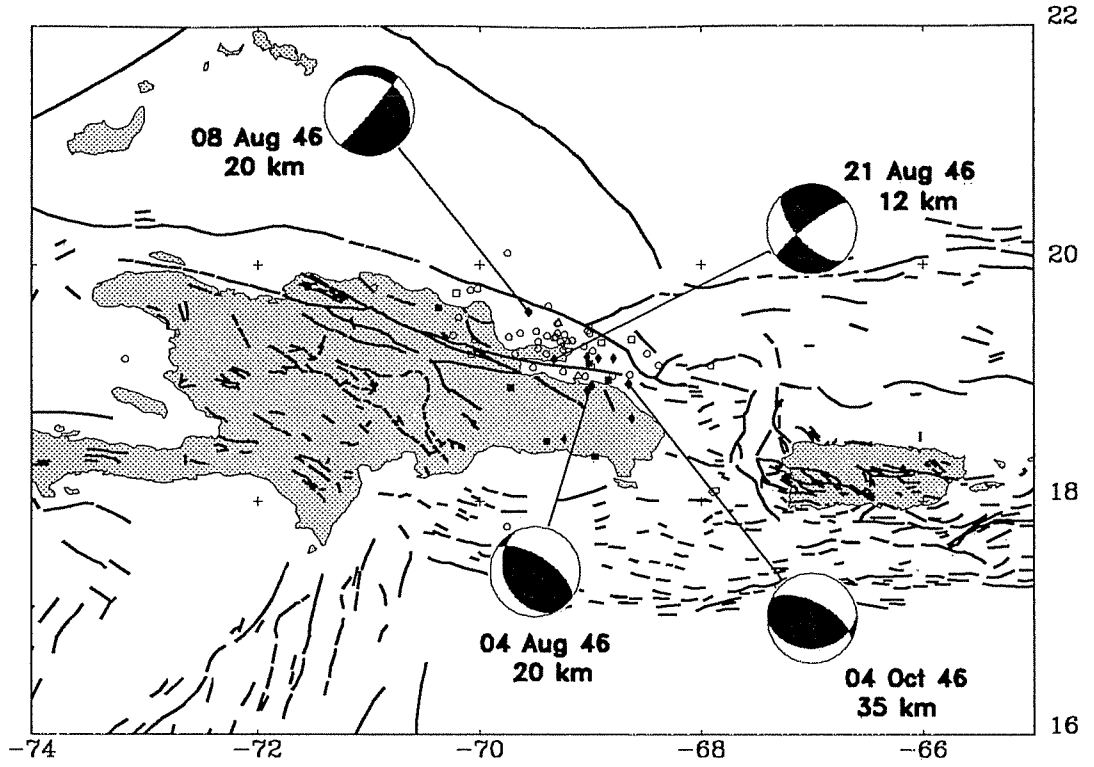

Figure 8. Focal mechanisms (lower hemisphere) and relocated 1946 events superposed on mapped faults. Note the mechanisms all have a nodal plane striking NW or WNW, approximately parallel the Septentrional Fault Zone and other faults.

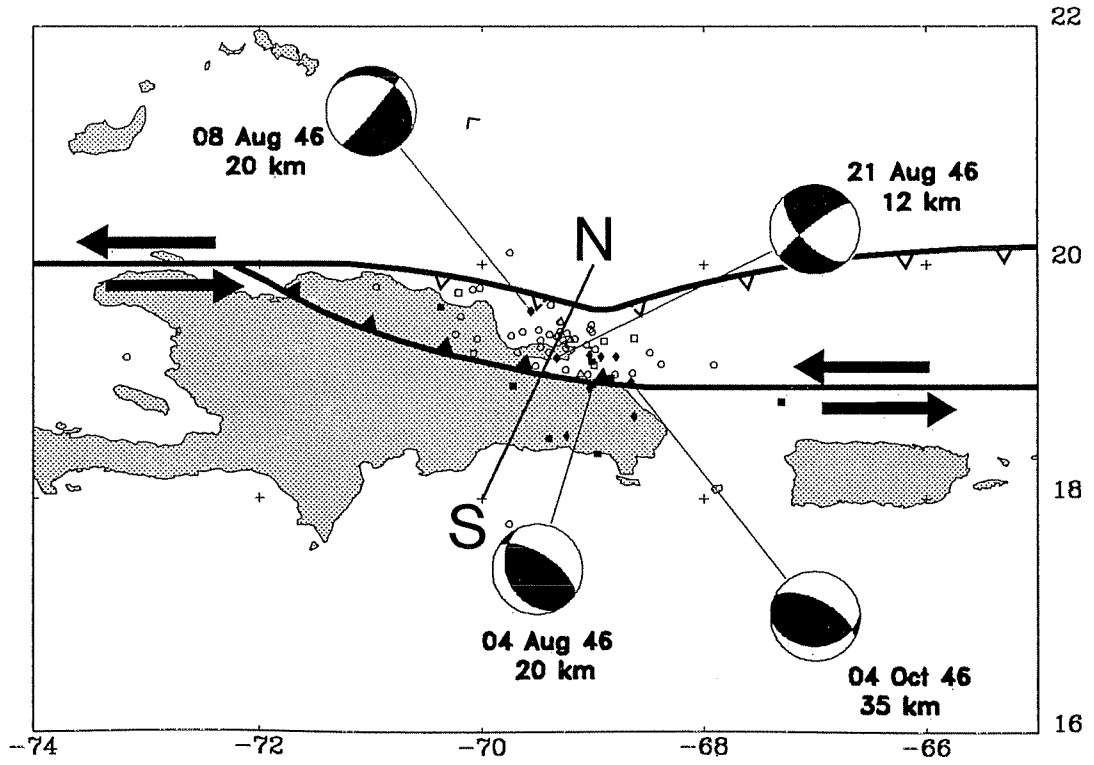

Figure 9a. Schematic interpretation of 1946 earthquakes as motions on a restraining bend in NA-Ca plate boundary zone. Heavy lines, possible loci of significant NA-Ca motion; arrows give sense (left-lateral); teeth on restraining bend portion (solid) indicate sense of overriding; heavy line with open teeth is approximate lithospheric subduction trace of NA.

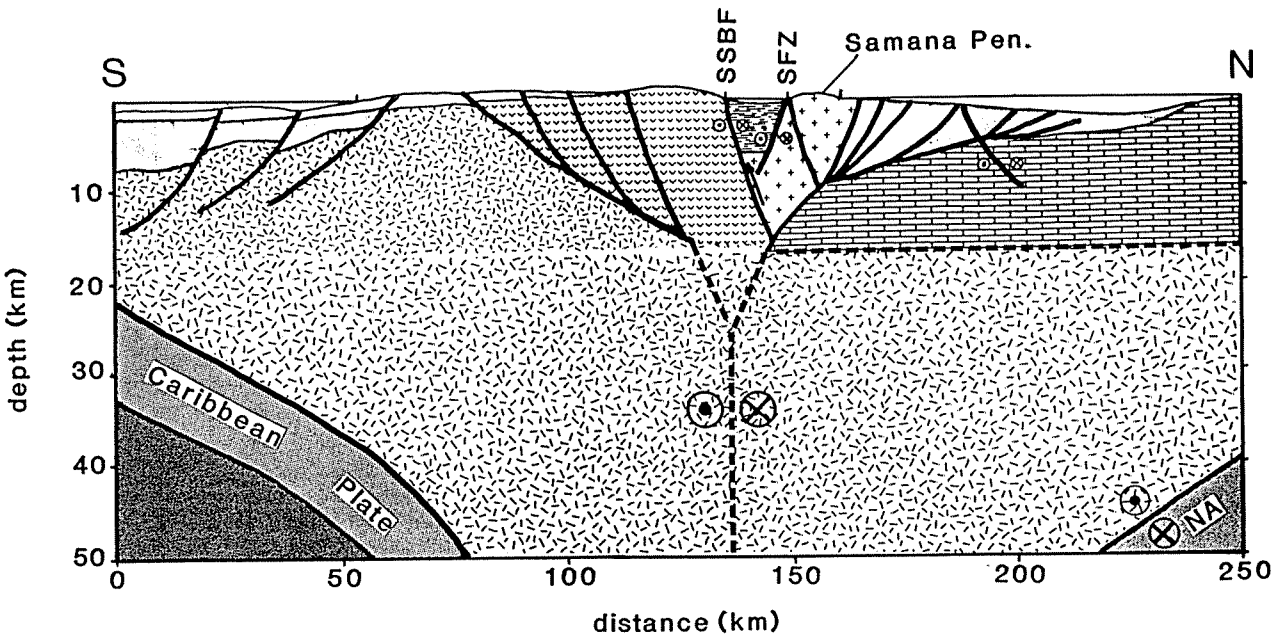

Figure 9b. Schematic cross section of plate boundary zone along line shown in Figure 9a. Heavy lines: faults; motion indicators on shallow faults show possible activity of 1946 earthquake series. Patterns: crosses, Septentrional and Samaná terrane; bricks, Bahamas Platform basement; dashed horizontal rule, Cibao Basin sediments. Possible motions at depth indicated. Geology based on *Lewis and Draper,* [1986].

part of the slipped region defined by the aftershocks, is thus representative of westward convergence at the restraining bend curve. The presumed fault plane of the main shock dips NE, and assuming that the fault plane of the October 4 event dips similarly, it is clear that the eastern side of the bend is thrust over the western side. Thus, it is possible that the Septentrional and Samaná terrane is overriding the Cibao Basin (Figure 9b). The NW trending left-lateral strike-slip at the NE end of the aftershock region may indicate that displacements are partitioned in the restraining bend. Alternatively, this strike-slip may indicate that the NW portion of the slipped region experiences differential motion as the faults curve away from the restraining bend. In fact, our preferred nodal plane for the August 8 event strikes nearer to west than does that of the more easterly August 21 event, perhaps indicative of the termination of the restraining bend as the principal displacement surfaces curve towards E-W trend. If this is so, the NW trend of these slip vectors may indicate that the curvature of faults exiting the restraining bend results in extension associated with such curvature that allows these motions. The SSW directed thrusting of the October 4 earthquake may indicate that there is a transpressive component to the plate boundary motions in eastern Hispaniola, or it may reflect stress refraction signifying a weak fault zone [*Mount and Suppe,* 1987] in the restraining bend. In either case, the October 4 event is consistent with the observation of south verging folded sediments in the Peninsula del Este terrane [*Lewis and Draper,* 1990] (see above).

Our interpretation that the 1946 events occurred on several faults in a restraining bend of the plate boundary zone has interesting implications. First, it is possible that active subduction of Caribbean lithosphere in the western Muertos Trough may be analogous to underthrusting of the Los Angeles basin beneath the Transverse ranges in southern California [*Hadley and Kanamori,* 1977; *Namson and Davis,* 1988; *Humphreys and Clayton,* 1990]. If southward subduction of North American lithosphere is also active, then given the northward dips of our preferred thrust fault planes, wedging of Hispaniola crust between this southward dipping slab and the overriding Septentrional-Samaná terrane is likely (Figure 9b), similar to the tectonic wedging model proposed by *Russo and Speed* [1992, 1994] for the eastern Caribbean-South America plate boundary zone.

Finally, because of the large magnitudes of the main shock and several of the 1946 series aftershocks, these events have important implications for NA-Ca plate boundary zone motions in the vicinity of Hispaniola. The slip vector of the magnitude 7.8 M_S August 4 event is probably the best gauge of the time-averaged terrane motion in this area. As we discuss above, the slip vector trends due west, consistent with left-lateral motion along E-W striking faults in the NA-Ca plate boundary zone. If the thrust motions delineated by the main shock and the October 4 event can be ascribed solely to the effects of a restraining bend in the plate boundary zone in eastern Hispaniola, then the motion of the Septentrional and Samaná terrane relative to the remainder of Hispaniola is largely devoid of extensile or compressive components normal to the plate boundary zone. However, the distribution of recent seismicity in this area (Figure 7) clearly demonstrates that motions

occur all along the southern coast of Hispaniola, and therefore, the island moves relative to the Caribbean plate. Thus, the motions of the Hispaniola terranes represented by the 1946 earthquakes cannot be extrapolated to encompass the full NA-Ca motion.

Historical Seismicity and Hazard

The preinstrumental historical record of seismicity has been summarized by *Scherer* [1912]. Large earthquakes occurred along the northwestern coast of the island in 1564, 1842, and 1887, and the southwestern and south central margin of the island also suffered violent earthquakes in 1751 (two), 1770, and 1860. Three of the latter events severely damaged Port-au-Prince, Haiti's capital city, and the fourth (first 1751 event) caused damage in Santo Domingo, capital of the Dominican Republic. The 1751, 1770, and 1842 earthquakes caused destructive and fatal tsunamis on both the northern and southern margins of Hispaniola. Thus, although the northwestern, southwestern, and south central margins of the island have been affected by large events, northeastern Hispaniola was quiescent until the 1946 earthquakes. Although the very early historical record is certainly incomplete, the uniqueness of the 1946 series in the available history may indicate very long recurrence times for northeastern Hispaniola.

Conclusions

The 1946 Hispaniola earthquakes occurred in a 75-km-wide elongate zone trending WNW, centered on the Samaná Peninsula of the eastern Dominican Republic. The earthquakes were both shallow (0 to 70 km) and intermediate (70 to 130 km) in depth, and the intermediate depth events may delineate a SSW dipping slab. The trend of the shallow aftershocks parallels tectonic terrane boundaries delineated by the strikes of mapped faults in the NA-Ca plate boundary zone, particularly the Septentrional Fault and the South Samaná Bay Fault. We believe the width of the shallow aftershock zone, in conjunction with the variability in preferred fault plane dip, indicates that the earthquakes occurred on several faults or splays.

Focal mechanisms of the main shock, August 4, 1946, ($M_S = 7.8$) and three large magnitude aftershocks (August 8, 1946, $M_S = 7.3$; August 21, 1946, $M_S = 6.2$; October 4, 1946, $M_S = 6.1$) include thrust and strike-slip motions. We interpret the events as displacements on a WNW trending restraining bend segment of the NA-Ca plate boundary zone. These motions include westward directed thrusting and left-lateral strike-slip on a NW striking plane for the main shock, left-lateral strike-slip on NW striking nodal planes for the two other August events, and SSW directed thrusting on a NW striking plane for the October 4 event. The variation in mechanisms may be a result of strain partitioning along the restraining bend segment or may arise from non-uniform slip of blocks in the restraining bend. Because of its large magnitude, we postulate that the main shock slip vector, trending due west, is the best available gauge of time-averaged motion between terranes in this portion of the NA-Ca plate boundary zone.

Acknowledgments. We thank Brad Gaynes and Carol Epling for their warm hospitality during the initial phase of this work. We thank Sean Solomon for facilitating A. V.'s sojourn at DTM. We thank Father James McCaffrey of the Weston Observatory, James Taggart and Miguel Benites of the NEIC, Josep Batlló of the Ebro Observatory, Teresa Susagna of the Fabra Observatory, and Don Schieman of the Department of Energy, Mines and Resources, Ottawa for providing us with high-quality data. David Wald provided us with SJG station parameters for August 1946. Arthur Snoke generously made available his program for evaluating focal mechanisms and came to our aid in dispelling important problems. We thank Bob Speed, Alan Linde, Selwyn Sacks, David Wald, and Diane Doser for thought-provoking discussion. We benefited from helpful reviews by Seth Stein, Albert Hsui, and an anonymous reviewer. This research was supported in part by the Generalitat de Catalunya, CIRIT, through grant EE93-62 to A. V.

References

Abe, K., Magnitudes of large shallow earthquakes from 1904 to 1980, *Phys. Earth Planet. Inter., 27,* 72-92, 1981.

Austin, J. A., OBC 5-A: Overthrusting in a deep-water carbonate terrane, *AAPG Stud. in Geol., 3*(15), 3.4.2-167-3.4.2-172, 1983.

Bjarnasson, I. Th., and P. Einarsson, Source mechanism of the 1987 Vatnafjöll earthquake in south Iceland, *J. Geophys. Res., 96,* 4313-4324, 1987.

Bowin, C., Geology of central Dominican Republic, Ph.D. thesis, 211 pp., Princeton Univ., Princeton, N.J., 1960.

Byrne, D. B., G. Suarez, and W. R. McCann, Muertos Trough subduction–Microplate tectonics in the northern Caribbean?, *Nature, 317,* 420-421, 1985.

Calais, E., N. Berthoux, and B. M. de Lepinay, From transcurrent faulting to frontal subduction: a seismotectonic study of the northern Caribbean plate boundary from Cuba to Puerto Rico, *Tectonics, 11,* 114-123, 1992.

Case, J. E., and T. L. Holcombe, Geologic tectonic map of the Caribbean region, *U.S. Geol. Surv. Misc. Invest. Map, I-1100,* 1980.

DeMets, C., R. G. Gordon, D. F. Argus, and S. Stein, Current plate motions, *Geophys. J. Int. 101,* 425-478, 1990.

Fischer, K. M., and W. R. McCann, Velocity modeling and earthquake relocation in the northeast Caribbean, *Bull. Seismol. Soc. Am., 74,* 1249-1262, 1984.

Geller, R. J., and H. Kanamori, Magnitudes of great shallow earthquakes from 1904 to 1952, *Bull. Seismol. Soc. Am., 67,* 587-598, 1977.

Grow, J. A., and R. E. Sheridan, U.S. Atlantic continental margin: A typical Atlantic-type or passive continental margin, in *The Geology of North America,* vol. I, *The Atlantic Continental Margin: U.S.,* edited by R. E. Sheridan and J. A. Grow, pp. 1-8, Geological Society of America, Boulder, Colo., 1988.

Gutenberg, B., and C. F. Richter, *Seismicity of the Earth and Associated Phenomena,* 2nd ed., 310 pp., Princeton University Press, Princeton, N.J., 1954.

Hadley, D., and H. Kanamori, Seismic structure of the Transverse Ranges, California, *Geol. Soc. Am. Bull., 88,* 1469-1478, 1977.

Helmberger, D. V., Generalized ray theory for shear dislocations, *Bull. Seismol. Soc. Am., 64,* 45-64, 1974.

Horsfield, W. T., Quaternary vertical movements in the Greater Antilles, *Geol. Soc. Am. Bull., 86,* 933-938, 1975.

Humphreys, E. D., and R. W. Clayton, Tomographic image of the southern California mantle, *J. Geophys. Res., 95,* 19,725-19,746, 1990.

Jordan, T. H., The present-day motions of the Caribbean plate, *J. Geophys. Res. 80,* 4433-4439, 1975.

Joyce, J., Blueschist metamorphism and deformation on the Samaná Peninsula: A record of subduction and collision in the Greater Antilles, in *Geologic and Tectonic Development of the North America-Caribbean Plate Boundary in Hispaniola,* edited by P. Mann, G. Draper, and J. F. Lewis, pp. 47-76, Geological Society of America, Boulder, Colo., 1991.

Kanamori, H., and G. Stewart, Mode of strain release along the Gibbs Fracture Zone, Mid-Atlantic Ridge, *Phys. Earth Planet. Int., 11,* 312-332, 1976.

Kisslinger, C., Evaluation of S to P amplitude ratios for determining focal mechanisms from regional network observations, *Bull. Seismol. Soc. Am., 70,* 999-1014, 1980.

Ladd, J. W., and J. S. Watkins, Active margin structures within the north slope of the Muertos trench, *Geol. Mijnbouw, 57,* 255-260, 1978.

Ladd, J. W., J. L. Worzel, and J. S. Watkins, Multifold seismic reflection records from the northern Venezuela basin and the north slope of the Muertos trench, in *Island Arcs, Deep Sea Trenches and Back Arc Basins, Maurice Ewing Ser.,* vol. 1, edited by N. I. Talwani and W. C. Pitman, pp. 41-56, AGU, Washington D.C., 1977.

Ladd, J. W., T. C. Shih, and C. J. Tsai, Cenozoic tectonics of central Hispaniola and adjacent Caribbean Sea, *AAPG. Bull., 65,* 466-489, 1981.

Langston, C. A. and D. V. Helmberger, A procedure for modeling shallow dislocation sources, *Geophys. J. R. Astron. Soc., 42,* 117-130, 1975.

Lewis, J. F. and G. Draper, Geology and tectonic evolution of the northern Caribbean margin, in *The Geology of North America,* vol. H, *The Caribbean Region,* edited by G. Dengo and J. E. Case, pp. 77-140, Geological Society of America, Boulder, Colo., 1990.

Lynch, J. J. and R. R. Bodle, The Dominican earthquakes of August, 1946, *Bull. Seism. Soc. Am., 38,* 1-17, 1948.

Mann, P., K. Burke, and T. Matumoto, Neotectonics of Hispaniola: Plate motion, sedimentation, and seismicity at a restraining bend, *Earth Planet. Sci. Lett., 70,* 311-324, 1984.

Maurrasse, F. J.-M., J. Husler, G. Georges, R. Schmitt, and P. Damond, Upraised Caribbean sea floor below acoustic reflector B" at the Southern Peninsula of Haiti, *Geol. Mijnbouw, 58,* 71-83, 1979.

McCaffrey, R., G. Abers, and P. Zwick, Inversion of teleseismic body waves, in *Digital seismogram analysis and waveform inversion, IASPEI Software Library,* vol. 3, edited by W. H. K. Lee, Seismological Society of America, El Cerrito, Calif., 1991.

McCann, W. R., and W. D. Pennington, Seismicity, large earthquakes, and the margin of the Caribbean plate, in *The Geology of North America,* vol. H, *The Caribbean Region,* pp. 291-306, edited by G. Dengo and J. E. Case, Geological Society of America, Boulder, Colo., 1990.

Molnar, P., Gravity anomalies and the origin of the Puerto Rico Trench, *Geophys. J. R. Astron. Soc., 51,* 701-708, 1977.

Molnar, P., and L. R. Sykes, Tectonics of the Caribbean and Middle America regions from focal mechanisms and seismicity, *Geol. Soc. Am. Bull. 80,* 1639-1684, 1969.

Mount, V. S., and J. Suppe, State of stress near the San Andreas fault: Implications for wrench tectonics, *Geology, 15,* 1143-1146, 1987.

Nabalek, J., Determination of earthquake source parameters from inversion of body waves, Ph.D. thesis, Mass. Inst. of Technol., Cambridge, 1984.

Namson, J., and T. Davis, Structural transect of the western Transverse Ranges, California: Implications for lithospheric kinematics and seismic risk evaluation, *Geology, 16,* 675-679, 1988.

Russo, R. M., and R. C. Speed, Oblique collision and tectonic wedging of the South American continent and Caribbean terranes, *Geology, 20,* 447-450, 1992.

Russo, R. M., and R. C. Speed, Spectral analysis of gravity anomalies and the architecture of tectonic wedging, NE Venezuela and Trinidad, *Tectonics, 13,* 613-622, 1994.

Russo, R. M., E. A. Okal, and K. C. Rowley, Historical seismicity of the southeastern Caribbean and tectonic implications, *Pure Appl. Geophys., 139,* 87-120, 1992.

Scherer, J., Great earthquakes in the island of Haiti, *Bull. Seismol. Soc. Am., 2,* 161-180, 1912.

Sheridan, R. E., H. T. Mullins, J. A. Austen, M. M. Ball, and J. W. Ladd, Geology and Geophysics of the Bahamas, in *The Geology of North America,* vol. I, *The Atlantic Continental Margin: U.S.,* edited by R. E. Sheridan and J. A. Grow, pp. 329-386, Geological Society of America, Boulder, Colo., 1988.

Snoke, J. A., J. W. Munsey, A. G. Teague, and G. A. Bollinger, A program for focal mechanism determination by combined use of polarity and $SV - P$ amplitude ratio data, *Earthquake Notes, 55,* 15, 1984.

Speed, R. C. and D. K. Larue, Extension and transtension in the plate boundary zone of the northeastern Caribbean, *Geophys. Res. Lett., 18,* 573-576, 1991.

Stein, S., C. DeMets, R. G. Gordon, J. Brodholt, D. Argus, J. F. Engeln, P. Lundgren, C. Stein, D. A. Wiens, and D. F. Woods, A test of alternative Caribbean plate relative motion models, *J. Geophys. Res., 93,* 3041-3050, 1988.

Sykes, L. R., W. R. McCann, and A. L. Kafka, Motion of Caribbean plate during last 7 million years and implications for earlier Cenozoic movements, *J. Geophys. Res., 87,* 656-676. 1982.

Talwani, M., G. H. Sutton, and J. L. Worzel, A crustal section across the Puerto Rico trench, *J. Geophys. Res., 64,* 1545-1555, 1959.

van der Hilst, R. D., Tomography with P, PP and pP delay-time data and the three-dimensional mantle structure below the Caribbean region, Ph.D. thesis, 250 pp., Univ. of Utrecht, 1990.

Vanek, J., A. Zatopek, V. Karnik, N. V. Kondorskaya, Y. V. Riznichenko, E. F. Savarensky, S. L. Solov'ev, and N. V. Shebalin, Standardization of magnitude scales, *Izv. Akad. Nauk S.S.S.R., Ser. Geofiz., 2,* 153-158, 1962.

Wysession, M. E., E. A. Okal, and K. L. Miller, Intraplate seismicity of the Pacific basin, *Pure Appl. Geophys., 135,* 261-359, 1991.

R. M. Russo, Laboratoire de Tectonophysique, Université de Montpellier II, Place Eugene Bataillon, 34095 Montpellier, CEDEX 05 France. (email: russo@lake.ciw.edu)

A. Villaseñor, Instituto de Ciencias de la Tierra (Jaume Almera), Martí i Franques, s/n, 08028 Barcelona, Spain.

(Received January 14, 1994; revised September 22, 1994; accepted September 29, 1994.)